AIP Journal of Applied Physics

# Silver migration and trapping in ion implanted ZnO single crystals

Alexander Azarov, Lasse Vines, Protima Rauwel, Edouard Monakhov, and Bengt G. Svensson

Citation: Journal of Applied Physics **119**, 185705 (2016); doi: 10.1063/1.4949331
View online: http://dx.doi.org/10.1063/1.4949331
View Table of Contents: http://scitation.aip.org/content/aip/journal/jap/119/18?ver=pdfcov
Published by the AIP Publishing

**Articles you may be interested in**

Effect of implanted species on thermal evolution of ion-induced defects in ZnO
J. Appl. Phys. **115**, 073512 (2014); 10.1063/1.4866055

Defect formation and thermal stability of H in high dose H implanted ZnO
J. Appl. Phys. **114**, 083111 (2013); 10.1063/1.4819216

Defects in N, O and N, Zn implanted ZnO bulk crystals
J. Appl. Phys. **113**, 103509 (2013); 10.1063/1.4795261

Structural and photoluminescence properties of Gd implanted ZnO single crystals
J. Appl. Phys. **110**, 033534 (2011); 10.1063/1.3619852

Annealing process of ion-implantation-induced defects in ZnO: Chemical effect of the ion species
J. Appl. Phys. **99**, 093507 (2006); 10.1063/1.2194113

Reuse of AIP Publishing content is subject to the terms at: https://publishing.aip.org/authors/rights-and-permissions. Download to IP: 129.240.205.39 On: Mon, 11 Jul 2016 12:26:05

JOURNAL OF APPLIED PHYSICS **119**, 185705 (2016)

# Silver migration and trapping in ion implanted ZnO single crystals

Alexander Azarov, Lasse Vines, Protima Rauwel, Edouard Monakhov, and Bengt G. Svensson
*Department of Physics, Centre for Materials Science and Nanotechnology, University of Oslo, P.O. Box 1048 Blindern, N-0316 Oslo, Norway*

(Received 2 March 2016; accepted 29 April 2016; published online 13 May 2016)

Potentially, group-Ib elements (Cu, Ag, and Au) incorporated on Zn sites can be used for p-type doping of ZnO, and in the present paper, we use ion implantation to introduce Ag atoms in wurtzite ZnO single crystals. Monitoring the Li behavior, being a residual impurity in the crystals, as a tracer, we demonstrate that Zn interstitials assist the Ag diffusion and lead to Ag pile-up behind the implanted region after annealing above 800 °C. At even higher temperatures, a pronounced Ag loss from the sample surface occurs and concurrently the Ag atoms exhibit a trap-limited diffusion into the crystal bulk with an activation energy of ~2.6 eV. The dominant traps are most likely Zn vacancies and substitutional Li atoms, yielding substitutional Ag atoms. In addition, formation of an anomalous multipeak Ag distribution in the implanted near-surface region after annealing can be attributed to local implantation-induced stoichiometry disturbances leading to trapping of the Ag atoms by O and Zn vacancies in the vicinity of the surface and in the end-of-range region, respectively. *Published by AIP Publishing*. [http://dx.doi.org/10.1063/1.4949331]

## I. INTRODUCTION

ZnO is a wide and direct band gap semiconductor with numerous potential applications for next generation of opto-electronic devices working in the short (ultra-violet) wavelength region.[1] However, a true realization of bipolar ZnO-based devices is hindered by the well-known doping asymmetry issue, typical for II-VI semiconductors.[2] Indeed, similar to other II-VI semiconductors, ZnO can be readily doped n-type, while a stable and reproducible p-type doping is still lacking. The difficulties of p-type doping are usually attributed to low dopant solubility, lack of dopants having a shallow acceptor level, compensation by spontaneously formed intrinsic defects (hole killers) such as zinc interstitials ($Zn_i$) and oxygen vacancies ($V_O$), interaction with impurities, or self-compensation effects.[2,3] The research activity on p-type doping of ZnO is mainly focusing on the group-V atoms[4–6] as possible O-substituting elements or Zn substituting group-Ia elements.[7] Recently, it was theoretically predicted that group-Ib elements (Cu, Ag, and Au) incorporated on Zn site have a potential for p-type doping, where $Ag_{Zn}$ is the most promising candidate as shallow acceptor with an ionization energy of ~0.2–0.4 eV.[8,9] In fact, a weak p-type conductivity has been demonstrated for Ag doped ZnO film prepared by pulsed laser deposition.[10,11]

Alternatively, Ag can be introduced via ion implantation, and channeling emission studies have demonstrated that an Ag fraction of ~30% is incorporated on Zn site already in the as-implanted state for a dose of $2 \times 10^{13}$ cm$^{-2}$ at room temperature.[12] Despite that ion implantation has a number of advantages over alternative doping methods (e.g., thermal diffusion), formation and evolution of ion-induced defects affect the dopant distribution and the final atomic configuration(s). It has been demonstrated previously that dopant-defect reactions dominate both disorder formation and crystal recovery in ZnO for many different ion species.[13–17] Specifically, for Ag an enhanced concentration of extended defects, such as stacking faults, has been observed in ZnO single crystals.[17] Furthermore, the behavior of group Ia residual impurities in ZnO, such as Li, strongly depends on the implanted species and the kinetics of defect annealing. In fact, monitoring of the Li distribution can be used to follow the evolution of point defects[18] and as shown in Ref. 19, the Li atoms in n-type hydrothermally (HT) grown ZnO samples reside exclusively on substitutional Zn sites ($Li_{Zn}$).

In the present paper, we address the distribution of implanted Ag ions in the course of post-implantation annealing concurrent with that of residual Li atoms. It is demonstrated that the Ag atoms exhibit a trap-limited diffusion into the crystal bulk with an activation energy of ~2.6 eV, and that a loss of Ag atoms occurs through the surface at temperatures >850 °C. Further, evidence for incorporation of Ag atoms on Zn site is given where the atomic configuration is energetically favorable with a high thermal stability (≥1050 °C).

## II. EXPERIMENTAL

HT grown wurtzite ZnO single crystals of n-type, having a homogeneous distribution of residual Li impurities on the level of 3–5 $\times 10^{17}$ cm$^{-3}$, were implanted at room temperature with 500 keV Ag ions to a dose of $5 \times 10^{15}$ cm$^{-2}$. The implantations were carried out in the [0001] aligned direction. After implantation, the samples were isochronally annealed for 30 min in air at temperatures between 700 and 1150 °C.

The Ag and Li concentration versus depth profiles were measured by secondary ion mass spectrometry (SIMS) with a Cameca IMS 7f microanalyzer using 10 keV $O_2^+$ ions as the primary beam for the analysis. The intensity-concentration calibration was performed using as-implanted reference samples. The conversion from sputtering time to sample depth was performed by measurement of the crater depth using a



Reuse of AIP Publishing content is subject to the terms at: https://publishing.aip.org/authors/rights-and-permissions. Download to IP: 129.240.205.39 On: Mon, 11 Jul 2016 12:26:05

Dektak 8 stylus profilometer and assuming a constant erosion rate with time. As-implanted samples were also studied by transmission electron microscopy (TEM) to characterize the defect microstructure. The TEM specimens were prepared by mechanical thinning followed by 4 keV Ar-ion milling for approximately 30 min at room temperature. Cross-sectional imaging was carried out along the $[11\bar{2}0]$ zone axis using a JEM2010F microscope operating at 200 kV.

## III. RESULTS AND DISCUSSION

The behavior of the Ag atoms in the implanted samples annealed at moderate temperatures (700–850 °C) is illustrated in Fig. 1, showing (a) Ag and (b) Li concentration versus depth profiles. The Ag atoms display only a minor redistribution below 800 °C, while an unexpected pile-up occurs at ~2 $\mu$m after 800 °C. Concurrently, Li exhibits depletion, and the position of the Ag pile-up corresponds closely to the deep edge of the Li depleted region (Fig. 1(b)). Increase of the temperature to 850 °C leads to a shift of the Ag pile-up to ~3.5 $\mu$m and a kink in the Li profile is clearly visible at the same depth, despite that the Li atoms start to diffuse back toward the surface at this temperature. Note that the formation of a Li depleted region beyond the implanted peak is typical for Zn-substituting elements.[18] The mechanism of Li redistribution is related to fast moving interstitial Li ($Li_i$) formed via a kick-out reaction with Zn interstitials ($Zn_i$) emitted from the implanted region, i.e., $Zn_i + Li_{Zn} \rightarrow Zn_{Zn} + Li_i$. The $Zn_i$ excess needed for this reaction depends on the incorporation of the implanted elements on Zn sites. In its turn, the $Zn_i$ flux is determined by the annealing kinetics of the implantation-induced defects and the Ag pile-up can be attributed to a competition between Zn and Ag atoms to occupy Zn substitutional sites. $Zn_{Zn}$ has a lower total energy as compared with $Ag_{Zn}$, and $Ag_i$ redistributes to the end of the region exposed to the flux of $Zn_i$'s, as corroborated by the corresponding Li profiles.[20] The depth of the Ag pile-up remains almost unchanged after annealing between 850 and 1000 °C (see Figs. 1(a) and 2(a)), implying that the source of implantation-induced $Zn_i$'s is exhausted. It should be underlined that the Ag pile-up is stable at least up to 1000 °C, while at higher temperatures the peak is not resolved due to overlap with the ordinary Ag diffusion profile, discussed below. Accordingly, the Ag pile-up provides evidence for a $Ag_{Zn}$ configuration of high thermal stability.

In this context, it can be underlined that, in general, the Li depletion does not mean that a major fraction of the implanted atoms reside on truly substitutional Zn sites. For instance, formation of stable impurity-Zn vacancy complexes in the implanted region can affect the excess of $Zn_i$'s, and therefore, the Li depletion can develop even for low truly substitutional fractions of the implanted atoms. In addition, the Li depletion observed in the present work for Ag is weak as compared with other Zn-substitutional elements, such as P or B (Refs. 17 and 18), where the Li depletion can extend up to 10–30 $\mu$m below the surface. The relatively modest Li redistribution for Ag may indicate a low Zn

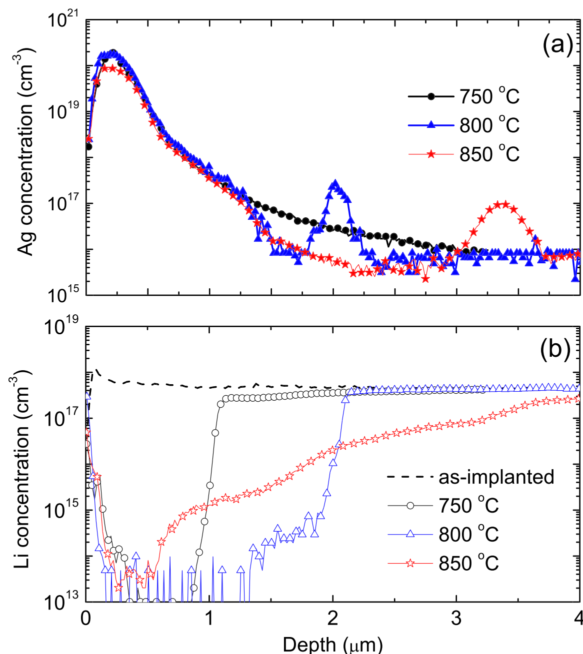


FIG. 1. (a) Ag and (b) corresponding Li concentration vs. depth profiles as measured by SIMS in ZnO samples implanted with Ag ions at room temperature and then annealed as indicated in the legend.

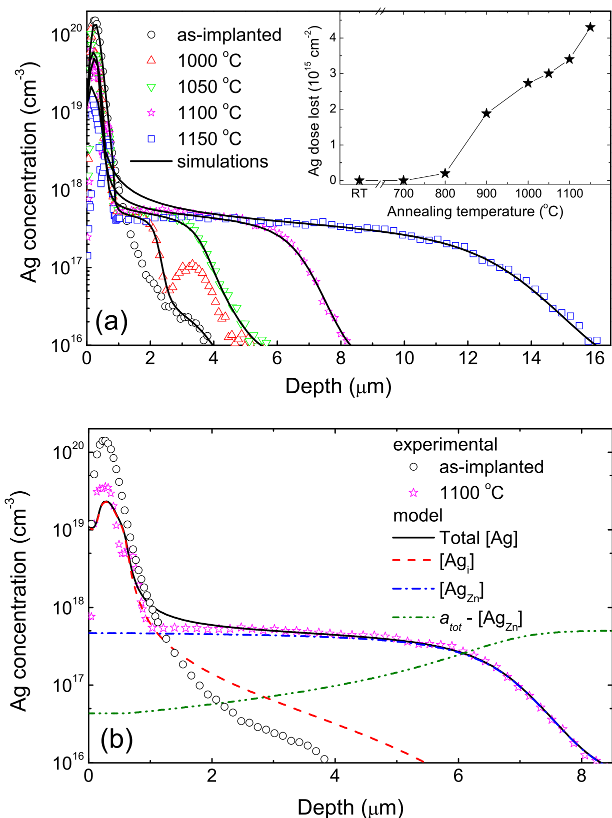


FIG. 2. (a) Ag concentration vs. depth profiles as measured by SIMS in ZnO implanted with Ag ions before and after annealing as indicated in the legend, and the corresponding simulated diffusion profiles assuming a trap-limited process (lines). The fraction of lost Ag dose as a function of the annealing temperature is shown in the inset. (b) Modeling results for the 1100 °C Ag profile illustrating the separate contributions of free ($Ag_i$) and trapped silver atoms ($Ag_{Zn}$) to the total Ag concentration (shown by the solid line). The concentration vs. depth profile of empty traps is also shown by the dashed dotted dotted line.

Reuse of AIP Publishing content is subject to the terms at: https://publishing.aip.org/authors/rights-and-permissions. Download to IP: 129.240.205.39 On: Mon, 11 Jul 2016 12:26:05

substitutional fraction of Ag in the implanted region and/or inefficient $Zn_i$ injection during the post-implant annealing.

Fig. 2 shows the concentration of Ag versus depth after heat treatments between 1000 and 1150 °C. The migration of Ag is revealed as a shoulder on the deep side of the implantation peak. The shoulder exhibits a concentration plateau of $\sim 5 \times 10^{17}\,cm^{-3}$ and its extension increases with increasing annealing temperature. This diffusion behavior is characteristic of a trap and solubility limited process, similar to that for hydrogen in ZnO,[21] where the concentration of Ag in the plateau region indicates a low solid solubility. Further, the descending slope at the end of the profile decreases with temperature, implying an increasing dissociation rate of trapped Ag atoms. A small decrease in the Ag concentration can also be observed at the shoulder after 1150 °C, suggesting a reduction in the trap concentration and/or a high dissociation rate of the trapped Ag atoms. It can be noted that trap limited diffusion is rather commonly observed in HT grown ZnO samples and has previously been reported for H,[21] Na,[23] Ga,[24] and In.[25] It was suggested in Ref. 23 that both the zinc vacancy and substitutional $Li_{Zn}$ can act as traps for interstitially migrating elements. In fact, the redistribution of Ag observed in Fig. 1(a) during injection of $Zn_i$'s provides strong evidence that a substitutional configuration ($Ag_{Zn}$) is energetically preferable, as also corroborated by modeling results.[20] Furthermore, the similar values of the Li bulk concentration and that of Ag in the diffusion shoulders in Fig. 2 indicate that ($Ag_{Zn} + Li_i$) has a lower total energy than ($Ag_i + Li_{Zn}$) and that the exchange occurs via a kick-out reaction of $Li_{Zn}$ with the migrating $Ag_i$'s.

Accordingly, a trap and solubility limited diffusion model has been applied, described by the following set of partial differential equations:[21]

$$\frac{\partial[Ag_i]}{\partial t} = D\frac{\partial^2}{\partial x^2}[Ag_{SS}] - \frac{\partial[Ag_{Zn}]}{\partial t},$$
$$\frac{\partial[Ag_{Zn}]}{\partial t} = k[Ag_{SS}](a_{tot} - [Ag_{Zn}]) - \nu[Ag_{Zn}],$$
$$[Ag_{SS}] = \frac{SS}{[Ag_i] + SS}[Ag_i], \tag{1}$$

where $[Ag_i]$ is the total concentration of free Ag atoms provided by the implanted diffusion source, $t$ is the annealing time, $x$ is the sample depth, and $D$ is the $Ag_i$ diffusion coefficient. $[Ag_{SS}]$ is the actual concentration of the $Ag_i$ atoms able to migrate into the sample which is assumed to be limited by the solid solubility ($SS$) of $Ag_i$. $[Ag_{Zn}]$ denotes the concentration of trapped Ag atoms, and $a_{tot}$ is the total concentration of traps. The kinetic coefficients $k = 4\pi RD$ ($R$ is a capture radius between the $Ag_i$ atoms and the traps) and $\nu$ are the trapping rate of $Ag_i$ atoms and dissociation rate of $Ag_{Zn}$, respectively. The total Ag concentration at a given time is the sum of $[Ag_i]$ and $[Ag_{Zn}]$. All the as-implanted Ag atoms are assumed to be free ($Ag_i$), and the as-implanted Ag concentration vs. depth profile is used as the initial condition ($t = 0$). In the simulations (the results are shown by the solid lines in Fig. 2(a)), the $Ag_i$ solid solubility was kept fixed at $5 \times 10^{16}\,cm^{-3}$,[22] while the trap concentration was put to $5 \times 10^{17}\,cm^{-3}$, i.e., similar to the bulk Li concentration, except for the 1150 °C sample (see discussion above) where it was estimated to be $\sim 4 \times 10^{17}\,cm^{-3}$. For $R$, a geometrical value of 5 Å was used. For clarity, the individual contributions of the free ($Ag_i$) and trapped ($Ag_{Zn}$) Ag atoms to the total Ag concentration are shown in Fig. 2(b) where the concentration of empty traps ($a_{tot} - [Ag_{Zn}]$) is also plotted. The $Ag_{Zn}$ atoms dominate in the diffusion shoulder, while $Ag_i$ prevails in the implantation peak.

Fig. 3 shows the Arrhenius plots of $D$ and $\nu$ deduced from the simulations. Note that the largest uncertainty in the $D$ and $\nu$ values occur at the temperatures below 1050 °C where the pile-up profile overlaps partly with the tail of the "ordinary" diffusion profile. Assuming that the $\nu$ pre-exponential factor ($\nu_0$) reflects the attempt frequency for a dissociative process, typically in the range of $1 \times 10^{13}\,s^{-1}$, the activation energy for dissociation of the trapped Ag atoms becomes $3.7 \pm 0.2$ eV. In its turn, the value for the extracted activation energy and pre-exponential factor of $D$ are $2.6 \pm 0.1$ eV and $5 \pm 1\,cm^2/s$, respectively. The obtained activation energy for Ag diffusion is about 1 eV higher compared with that predicted theoretically based on first principle calculations using the generalized-gradient approximation with the functional of Perdew, Burke, and Ernzerhof.[20] The accuracy of the theoretical value in Ref. 20 is not known but it should be mentioned that our (ion-implanted) diffusion source may not be fully ideal with a limited release of $Ag_i$ atoms. As shown below, interaction between ion-induced defects and the implanted Ag atoms takes place even at high temperatures and an energy barrier for release of $Ag_i$ atoms trapped in the implanted region may account for the $\sim$1 eV larger activation energy of $D$ relative to the theoretical value. In addition, the anneals above 800 °C are accompanied by a loss of Ag atoms outdiffusion through the sample surface, as illustrated by the inset in Fig. 2. On the other hand, the density of Ag atoms in the implanted source is a factor of about 10 to 100 higher than that in the diffusion shoulder, in principle ensuring a sufficient supply of Ag atoms.

An intriguing interaction of the Ag atoms with the implantation-induced defects is revealed by Fig. 4, showing enlarged fragments of the Ag concentration vs depth profiles in the vicinity of the implantation peak. After 1000 °C, the Ag atoms exhibit three distinct peaks: close to surface ($\sim$100 nm), at the projected range ($\sim$220 nm), and in the

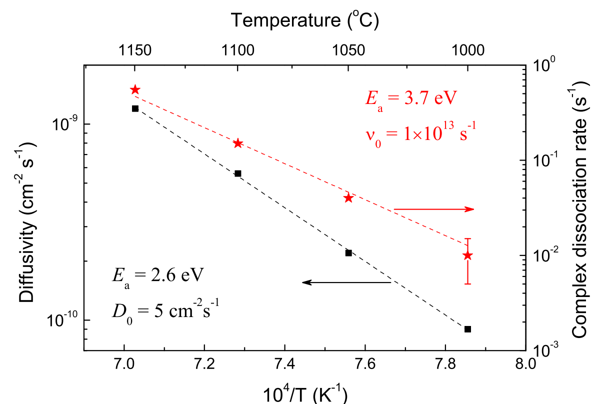


FIG. 3. Arrhenius plots of the extracted Ag diffusion constant (left-hand scale) and the dissociation rate of the trapped Ag atoms (right-hand scale) vs the reciprocal absolute temperature.

Reuse of AIP Publishing content is subject to the terms at: https://publishing.aip.org/authors/rights-and-permissions. Download to IP: 129.240.205.39 On: Mon, 11 Jul 2016 12:26:05

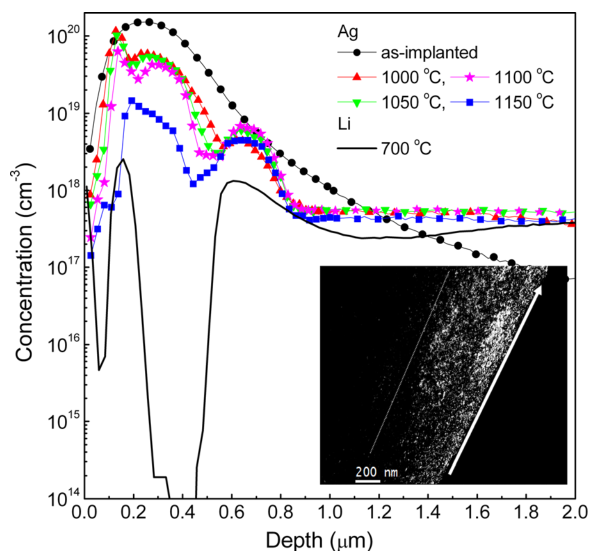


FIG. 4. Fragments of the Ag concentration vs. depth profiles shown in Fig. 2 illustrating anomalous redistribution in the vicinity of the implanted peak. The Li profile after 700 °C annealing is included for comparison (solid line). The inset shows the dark field (cross-sectional) TEM image of an as-implanted sample, where the thick white line indicates the sample surface and the thin dashed one indicates the end of the damaged region.

end-of-range region (∼650 nm). Annealing at higher temperature leads to some narrowing of the central peak and accumulation in the end-of-range region. At 1150 °C, a pronounced release of trapped Ag atoms occurs both at the near surface and at the central peak, while the end-of-range peak remains stable despite that the major part of ion-induced defects has disappeared at this temperature.[17]

Agglomeration and clustering of Ag atoms is expected around the projected range (the central peak) due to the high local concentration.[9] Further, according to the TEM results shown in the inset of Fig. 4, the damaged layer extends up to ∼600 nm in depth (indicated by the white dashed line) and consists of planar defects in addition to clusters of vacancies and/or interstitials, corroborated by previous studies of the defect microstructure in ZnO samples implanted by heavy ions.[17,28] The end-of-range Ag peak occurs in the transition region between the damaged layer and the crystalline sample bulk where the defect density is comparatively low. Interestingly, also the Li concentration vs depth profile after 700 °C annealing (shown by the solid line in Fig. 4) reveals accumulation at the depths corresponding to the near the surface and end-of-range Ag-peaks. As discussed above, open-volume defects are efficient traps for both Li and Ag, and they are a possible cause for the pile-up in both the near surface and end-of-range regions. An enhanced concentration of vacancy type defects at the both sides of the projected range can be attributed to a local stoichiometric imbalance in the collision cascades.[26,27] The calculations predict that such stoichiometric disturbances can be pronounced in heavy ion implanted compound semiconductors with a large mass ratio of the constituent elements. Excess of the heavier and lighter elements is expected to develop near the surface and at end-of-range regions, respectively.[26,27] Specifically for ZnO, this leads to a deficiency of oxygen (oxygen vacancies) at shallow depths and a deficiency of Zn ($V_{Zn}$'s) at depths beyond the projected range. Hence, the profiles in Fig. 4 suggest that the Ag atoms can be trapped forming stable $Ag_O$ and $Ag_{Zn}$ configurations near the surface and at the end-of-range, respectively. Furthermore, the results also indicate a lower thermal stability of $Ag_O$ as compared with $Ag_{Zn}$.

Finally, it should be mentioned that Yaqoob and Huang[29] addressed the diffusion of Ag (and In) in ion-implanted ZnO samples by monitoring the redistribution of Ag in the implantation peak region using Rutherford backscattering spectrometry (RBS) measurements. Consistent with our data, they found a complex interaction between the Ag atoms and the implantation-induced defects. Analysis of the RBS results led to somewhat contradictory conclusions, e.g., $Ag_i$ exhibited a fast diffusivity despite having a higher migration energy than $Ag_{Zn}$ and despite its low migration barrier (∼1.1 eV), $Ag_{Zn}$ displayed a high thermal stability. It was concluded in Ref. 29 that a more detailed study is required to understand the atomistic processes occurring in the implantation peak region.

## IV. CONCLUSIONS

In conclusion, injection of $Zn_i$'s from the implanted near-surface region at temperatures between ∼800 and 900 °C causes redistribution of the Ag atoms in the profile tail at large depths. Accumulation of the Ag atoms occurs at the maximum depth of the $Zn_i$ penetration, as monitored by Li as trace element; this is attributed to a competition between $Zn_i$ and $Ag_i$ to react with $V_{Zn}$'s or $Li_{Zn}$'s and occupy Zn substitutional sites. The migration of the Ag atoms is interstitial-assisted, and at high temperatures (≥1000 °C) when the supply of implantation-induced $Zn_i$'s is exhausted, the Ag atoms exhibit a trap-limited diffusion into the sample bulk with an activation energy of ∼2.6 eV. Dominant traps in HT grown material for the migrating $Ag_i$'s are most likely $Li_{Zn}$ and $V_{Zn}$. The substitutional $Ag_{Zn}$ configuration displays a high thermal stability with a dissociation energy barrier of ∼3.7 eV. Finally, in the implanted near-surface region an anomalous multipeak distribution of the Ag concentration evolves with the annealing temperature. This may be due to local implantation-induced stoichiometry perturbations, leading to trapping of the Ag atoms by oxygen vacancies, in the vicinity of the surface, and $V_{Zn}$'s, in the end-of-range region.

## ACKNOWLEDGMENTS

This work was performed within The Norwegian Research Centre for Solar Cell Technology (Project No. 460976), a Centre for Environment-friendly Energy Research cosponsored by the Norwegian Research Council and research and industry partners in Norway.

[1] Ü. Özgür, Y. I. Alivov, C. Liu, A. Teke, M. A. Reshchikov, S. Doğan, V. Avrutin, S.-J. Cho, and H. Morkoç, J. Appl. Phys. 98, 041301 (2005).
[2] C. H. Park, S. B. Zhang, and S.-H. Wei, Phys. Rev. B 66, 073202 (2002).
[3] S. B. Zhang, J. Phys.: Condens. Matter 14, R881 (2002).
[4] M. A. Myers, M. T. Myers, M. J. General, J. H. Lee, L. Shao, and H. Wang, Appl. Phys. Lett. 101, 112101 (2012).
[5] F. X. Xiu, Z. Yang, L. J. Mandalapu, D. T. Zhao, J. L. Liua, and W. P. Beyermann, Appl. Phys. Lett. 87, 152101 (2005).

Reuse of AIP Publishing content is subject to the terms at: https://publishing.aip.org/authors/rights-and-permissions. Download to IP: 129.240.205.39 On: Mon, 11 Jul 2016 12:26:05

[6]G. Braunstein, A. Muraviev, H. Saxena, N. Dhere, V. Richter, and R. Kalish, Appl. Phys. Lett. **87**, 192103 (2005).
[7]J. G. Lu, Y. Z. Zhang, Z. Z. Ye, Y. J. Zeng, H. P. He, L. P. Zhu, J. Y. Huang, L. Wang, J. Yuan, B. H. Zhao, and X. H. Li, Appl. Phys. Lett. **89**, 112113 (2006).
[8]Y. Yan, M. M. Al-Jassim, and S.-H. Wei, Appl. Phys. Lett. **89**, 181912 (2006).
[9]O. Volnianska, P. Boguslawski, J. Kaczkowski, P. Jakubas, A. Jezierski, and E. Kaminska, Phys. Rev. B **80**, 245212 (2009).
[10]H. S. Kang, B. D. Ahn, J. H. Kim, G. H. Kim, S. H. Lim, H. W. Chang, and S. Y. Lee, Appl. Phys. Lett. **88**, 202108 (2006).
[11]M. A. Myers, J. H. Lee, Z. Bi, and H. Wang, J. Phys.: Condens. Matter **24**, 145802 (2012).
[12]E. Rita, U. Wahl, A. M. L. Lopes, J. P. Araújo, J. G. Correia, E. Alves, J. C. Soares, and The ISOLDE Collaboration, Physica B **340–342**, 240 (2003).
[13]A. Yu. Azarov, E. Wendler, A. Yu. Kuznetsov, and B. G. Svensson, Appl. Phys. Lett. **104**, 052101 (2014).
[14]E. Sonder, R. A. Zhur, and R. E. Valiga, J. Appl. Phys. **64**, 1140 (1988).
[15]A. Yu. Azarov, B. G. Svensson, and A. Yu. Kuznetsov, Appl. Phys. Lett. **101**, 222109 (2012).
[16]Z. Q. Chen, M. Maekawa, A. Kawasuso, S. Sakai, and H. Naramoto, J. Appl. Phys. **99**, 093507 (2006).
[17]A. Yu. Azarov, A. Hallén, X. L. Du, P. Rauwel, A. Yu. Kuznetsov, and B. G. Svensson, J. Appl. Phys. **115**, 073512 (2014).
[18]A. Yu. Azarov, P. T. Neuvonen, K. E. Knutsen, L. Vines, B. G. Svensson, and A. Yu. Kuznetsov, Phys. Rev. Lett. **110**, 175503 (2013).
[19]K. M. Johansen, A. Zubiaga, I. Makkonen, F. Tuomisto, P. T. Neuvonen, K. E. Knutsen, E. V. Monakhov, A. Yu. Kuznetsov, and B. G. Svensson, Phys. Rev. B **83**, 245208 (2011).
[20]G.-Y. Huang, C.-Y. Wang, and J.-T. Wang, J. Phys.: Condens. Matter **21**, 345802 (2009).
[21]K. M. Johansen, J. S. Christensen, E. V. Monakhov, A. Yu. Kuznetsov, and B. G. Svensson, Appl. Phys. Lett. **93**, 152109 (2008).
[22]It should be noted that, in general, solid solubility limits of free ($Ag_i$) and trapped ($Ag_{Zn}$) atoms are different and in the present model we assume that the $Ag_{Zn}$ concentration does not affect the $Ag_i$ solubility. Moreover, despite that the $Ag_i$ solubility is a fitting parameter in the model, its upper limit cannot be higher than the Ag concentration in the plateau, i.e., $5 \times 10^{17}\,cm^{-3}$. In its turn, the data available in the literature on Ag solubility in ZnO is rather limited. In particular, it has been shown by first principle calculations that Ag doping limit is $\sim 10^{18}\,cm^{-3}$ at 700 °C for O-rich conditions; however, it could be significantly lower for Zn-rich conditions (Ref. 9).
[23]P. T. Neuvonen, L. Vines, V. Venkatachalapathy, A. Zubiaga, F. Tuomisto, A. Hallén, B. G. Svensson, and A. Yu. Kuznetsov, Phys. Rev. B **84**, 205202 (2011).
[24]T. Nakagawa, I. Sakaguchi, M. Uematsu, Y. Sato, N. Ohashi, H. Haneda, and Y. Ikuhara, Jpn. J. Appl. Phys., Part 1 **46**, 4099 (2007).
[25]T. Nakagawa, K. Matsumoto, I. Sakaguchi, M. Uematsu, H. Haneda, and N. Ohashi, Jpn. J. Appl. Phys., Part 1 **47**, 7848 (2008).
[26]L. A. Christel and J. F. Gibbons, J. Appl. Phys. **52**, 5050 (1981).
[27]R. E. Avila and C. D. Fung, J. Appl. Phys. **60**, 1602 (1986).
[28]J. D. Ye, S. Tripathy, F.-F. Ren, X. W. Sun, G. Q. Lo, and K. L. Teo, Appl. Phys. Lett. **94**, 011913 (2009).
[29]F. Yaqoob and M. Huang, in *MRS Proceedings of Oxide Semiconductors: Defects, Growth and Device Fabrication*, edited by T. Veal, S. Durbin, J. Phillips, M. Grundman (Cambridge University Press; Warrendale, PA, 2012), Vol. 1394.

Reuse of AIP Publishing content is subject to the terms at: https://publishing.aip.org/authors/rights-and-permissions. Download to IP: 129.240.205.39 On: Mon, 11 Jul 2016 12:26:05